ARTICLE

Tunable Stress and Controlled Thickness Modification in Graphene by Annealing

Zhen Hua Ni,[†,§] Hao Min Wang,[‡] Yun Ma,[†] Johnson Kasim,[†] Yi Hong Wu,[‡] and Ze Xiang Shen[†,*]

[†]Division of Physics and Applied Physics, School of Physical and Mathematical Sciences, Nanyang Technological University, 1 Nanyang Walk, Block 5, Level 3, Singapore 637616, [‡]Department of Electrical and Computer Engineering, National University of Singapore, 4 Engineering Drive 3, Singapore 117576, and [§]Department of Physics, National University of Singapore-2 Science Drive 3, Singapore 117542

ABSTRACT Graphene has many unique properties which make it an attractive material for fundamental study as well as for potential applications. In this paper, we report the first experimental study of process-induced defects and stress in graphene using Raman spectroscopy and imaging. While defects lead to the observation of defect-related Raman bands, stress causes shift in phonon frequency. A compressive stress (as high as 2.1 GPa) was induced in graphene by depositing a 5 nm SiO_2 followed by annealing, whereas a tensile stress (~0.7 GPa) was obtained by depositing a thin silicon capping layer. In the former case, both the magnitude of the compressive stress and number of graphene layers can be controlled or modified by the annealing temperature. As both the stress and thickness affect the physical properties of graphene, this study may open up the possibility of utilizing thickness and stress engineering to improve the performance of graphene-based devices. Local heating techniques may be used to either induce the stress or reduce the thickness selectively.

KEYWORDS: graphene · Raman · defects · stress · annealing.

Graphene, a monolayer graphite sheet, has attracted much interest since it was discovered in 2004.[1–3] The exceptionally high crystallization and unique electronic properties make graphene a promising candidate for ultra-high-speed nanoelectronics.[4] However, to make it a real technology, several critical issues need to be resolved which include but are not limited to (1) microelectronics compatible processes for fabricating both single layer and few layer graphene and related devices and (2) a viable way of creating an energy gap at *K* and *K*′ points in the Brillouin zone. Researchers have successfully developed an energy gap in graphene by patterning it into nanoribbon,[5] forming quantum dots,[4] or making use of mutilayer graphene sheets with or without the application of an external electrical field.[6,7] Besides global back gates,[8,9] top local gates[10–12] have also been employed to develop more complex graphene devices, such as pn junction,[13] Veselago lens,[14] and Klein tunneling.[15] The top-gate oxides that have been used so far include HfO_2, Al_2O_3, and SiO_2. Although efforts have been made to deposit the gate oxides without damaging the graphene or changing its electrical properties,[10–15] the gate oxides should influence the graphene sheets in at least three ways: doping, defects, and various mechanical deformations. Although theoretical studies suggest that chemical doping shifts the neutral point[1,16,17] and defects increase carrier scattering in graphene,[18,19] so far they have not been studied experimentally. It is known that the sp^2 bonds in graphitic carbon can hold extremely high mechanical strains[20] and exhibit interesting electromechanical properties, as observed in carbon nanotubes (CNTs).[21] Remarkable strain/stress effects on optical and electronic properties have been found in CNTs.[21–25] As both the CNTs and graphene share the same honeycomb structure,[26] it is plausible to expect a similar type of effects in graphene, especially in gapped structures such as graphene nanoribbon, quantum dot, and nanoconstrictions.

We have systematically studied graphene sheets subjected to defects and mechanical deformations induced by insulating capping layers using Raman spectroscopy and Raman microscopy. Different insulating materials were deposited on top of graphene by electron beam evaporation, pulsed laser deposition (PLD), and sputtering, followed by annealing at different temperatures. Here we present the results of using SiO_2 as a typical example. A thin layer of SiO_2 (5 nm) was deposited on top of the graphene sheets by PLD, and Raman spectroscopy was used to investigate the interaction between the SiO_2 and graphene. Defect-induced Raman bands were observed after the deposition of SiO_2. The amount of defects was significantly reduced by annealing. A striking feature in our spectroscopic data is that compressive stress as

*Address correspondence to zexiang@ntu.edu.sg.

Received for review January 16, 2008 and accepted April 10, 2008.

Published online May 1, 2008.
10.1021/nn800031m CCC: $40.75

© 2008 American Chemical Society

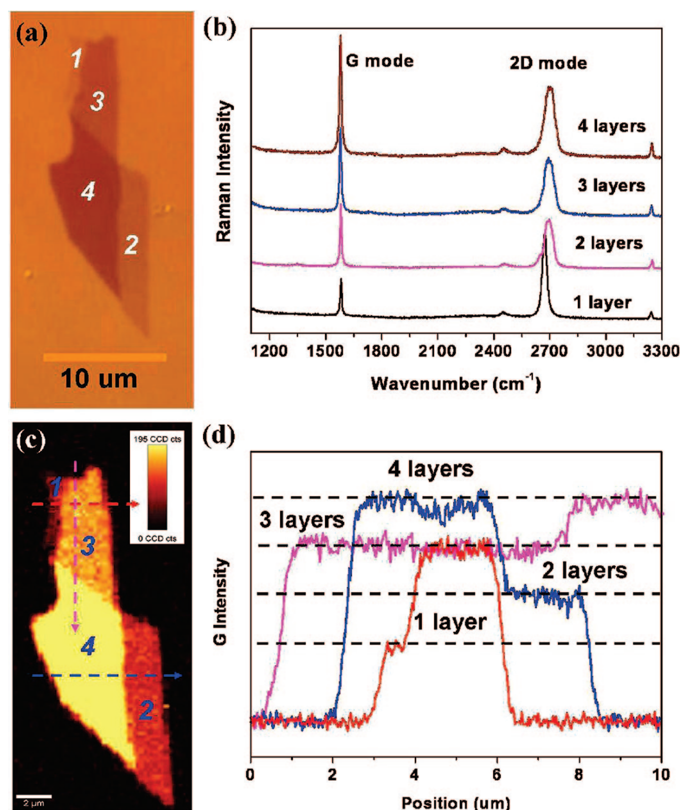

Figure 1. (a) Optical image of graphene with layers 1, 2, 3, and 4; (b) Raman spectra as a function of number of layers; (c) Raman image plotted by the intensity of G band; (d) the cross section of Raman image, which corresponds to the dash lines with corresponding colors in Raman image. It is obvious that the graphene sheet contains one, two, three, and four layers.

high as ~2.1 GPa was observed after the annealing process. The compressive stress may be useful to tune the electronic properties of graphene nanostructures. Possible applications to graphene-based devices and spectroscopic research are also presented. To the best of our knowledge, this is the first experimental report on defects and stress induced in graphene. We further show that the graphene thickness, and hence its properties, can be changed in a controlled manner by annealing in air.

RESULTS AND DISCUSSION

Figure 1a shows the optical image of a graphene sample on the SiO_2/Si substrate. The graphene sheet shows four different contrast regions, which can be attributed to four different thicknesses. The Raman spectra recorded from these regions are shown in Figure 1b. There are two intense features in the spectra, which are the in-plane vibrational (E_{2g}) G band and the two phonon 2D band, respectively. As has been proposed by Ferrari *et al.*[27] the second order Raman 2D band is sensitive to the number of layers of graphene and the 2D band of single layer graphene is very sharp and symmetric. In our Raman spectra, the sharp 2D band of the single layer graphene can be clearly observed and distinguished from bilayer and few-layer graphenes. We can further identify the thickness of other layers from the G band intensity plot, as shown in Figure 1c, since the intensity of G band increases almost linearly with the number of layers for few-layer graphene samples.[28] Figure 1d plots the Raman intensity of the G band along three dash lines drawn in Figure 1c. It is obvious that the graphene sheet contains one, two, three, and four layers.

The Raman spectra of graphene before and after 5 nm SiO_2 deposition were shown in Figure 2a. A clear difference is that two extra Raman bands, located at 1350 and 1620 cm^{-1}, were observed after deposition. Those two Raman bands were both defects induced: The stronger one at 1350 cm^{-1} is assigned to the so-called disorder-induced D band, which is activated by a double resonance effect by defects, such as in-plane substitutional heteroatoms, vacancies, or grain boundaries.[29] The weaker band at 1620 cm^{-1} is assigned to D′ band. The D′ band corresponds to the highest frequency feature in the density of state, which is forbidden under defect-free conditions.[30] Its observation is also associated with the presence of defects in the lattice and originates from the double resonance process. The observation of D and D′ bands indicate that defects were introduced into graphene after the 5 nm SiO_2 top layer deposition. This may be caused by the damage on the sample during deposition, or by the interaction between SiO_2 and graphene which may produce vacancy, dislocation, and/or dangling bonds. Annealing is carried out to eliminate the defects, which will be discussed in a later section. Figure 2b shows the Raman spectra of a graphene sheet with one to four layers as well as that of bulk graphite after SiO_2 deposition. The Raman spectra were taken under same conditions. The D band intensity decreases with the increase of graphene thickness and is invisible for bulk graphite, demonstrating that defects are more easily introduced into thinner graphene sheets.[31] Figure 2 panels c and e show Raman images generated from the intensity of D band before and after deposition, respectively. Before deposition, there is no D band hence the Raman image is dark. After deposition, the thinner graphene (single layer graphene) shows the strongest D band, which is consistent with the discussion above. Figure 3 panels d and f show the images generated from the intensity of the corresponding G band, and they do not show noticeable difference. Hence the G band intensity is still a good criterion in determining the thickness of the graphene sheet.

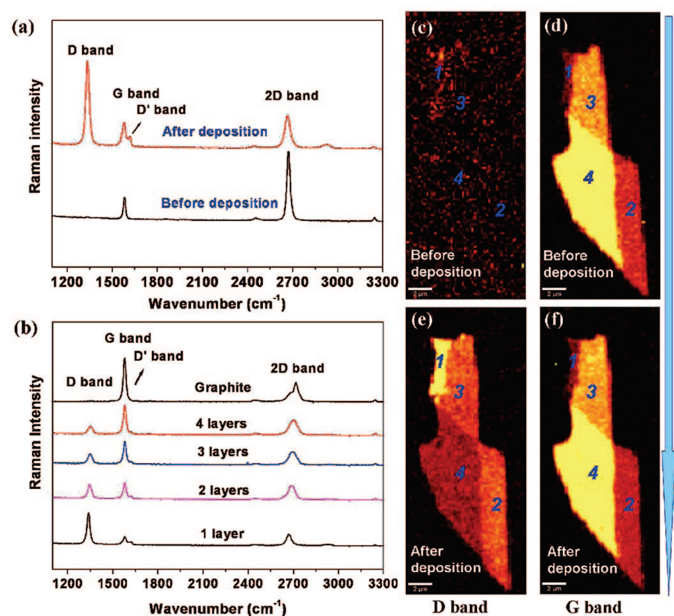

Figure 2. (a) Raman spectra of single layer graphene before and after the 5 nm SiO_2 deposition. (b) Raman spectra of graphene with different thicknesses as well as that of bulk graphite after 5 nm SiO_2 deposition. Raman images of graphene sheets before SiO_2 deposition generated from the intensity of the D band (c) and G band (d). Raman images of graphene sheets after 5 nm SiO_2 deposition using the intensity of D band (e), and G band (f). The thinner graphene sheets have stronger D band, hence they contain more defects.

We have also deposited different materials as capping layers with different methods as shown in Figure 3. SiO_2 layers were deposited with different methods: electron beam evaporation, PLD and RF sputtering. Different amounts of defects were introduced into the graphene sheets, as indicated by the relative intensity of the defect-induced D band. After HfO_2 thin layer deposition by PLD, strong defect-induced D band was observed. However, after polymethyl methacrylate (PMMA) deposition by spin coating, no change in Raman features was observed, as shown in Figure 3. Our results show that the deposition methods have a significantly effect on the defects, with spin coating introducing the least amount of defects and PLD and RF sputtering the most defects.

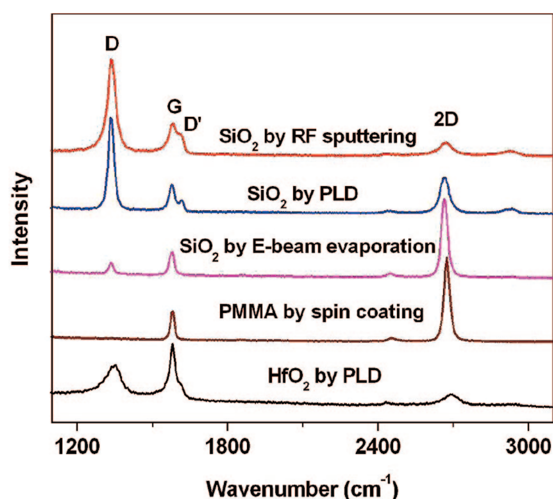

Figure 3. Raman spectra of graphene after SiO_2 deposition by RF sputtering, PLD, and e-beam evaporation as well as graphene after PMMA deposition by spin coating and HfO_2 deposition by PLD.

The Raman spectra of single layer graphene after annealing in air ambient at different temperatures are shown in Figure 4a. We have also carried out vacuum annealing and similar results were observed. An obvious observation is that the intensity of D band decreases upon annealing. This is clearly demonstrated in Figure 4b, which shows the intensity ratio between the D band and G band (I_D/I_G) that is often used to estimate the amount of defects in carbon materials. For one- to four-layer graphene sheets, this ratio decreases with increase in annealing temperature. This can be understood as due to the recovery of damaged graphene at high temperature. Figure 5a−c show another important observation, where the G, D, and 2D bands shifted to higher frequency with an increase in annealing temperature. The G band blue-shifted ~15 cm^{-1}, while the D band blue-shifted ~13 cm^{-1} and 2D band ~25 cm^{-1} after annealing at 500 °C. We attribute this significant blueshift of Raman bands to the strong compressive stress on graphene. The SiO_2 becomes denser upon anneal so it exerted a strong compressive stress on the graphene. For comparison, the Raman bands of bulk graphite did not shift after deposition and annealing, which supported the above explanation, as bulk graphite is too thick and it is not easily compressed by SiO_2. Recently, Yan *et al.*[32] and Pisana *et al.*[33] found that the frequency of the G and 2D Raman bands can also be adjusted by charge doping through electron−phonon coupling change. Besides the G band blueshift, a bandwidth narrowing of ~10 cm^{-1} was also observed in the case of charge doping. However, in our results, only a small fluctuation (±1 cm^{-1}) of G band fwhm (full width at half-maximum) was observed after annealing at different temperature, which indicates that the effect of charge doping can be ignored. In addition, it is shown that the dependence of the 2D band blueshift on doping is very weak and only −10 to 30% compared to that of G band.[32,34] Hence, the 25 cm^{-1} 2D band blueshift is too large to be achieved by charge doping alone. Therefore, the observed shifts of G (~15 cm^{-1}) and 2D (~25 cm^{-1}) band in our experiment were mainly caused by stress.

The compressive stress on graphene in our experiment is due to the denser of SiO_2 upon annealing. This origin of the compressive stress is very similar to the biaxial stress due to the lattice mismatch at the sample/substrate interface in a normal thin film. Therefore, the

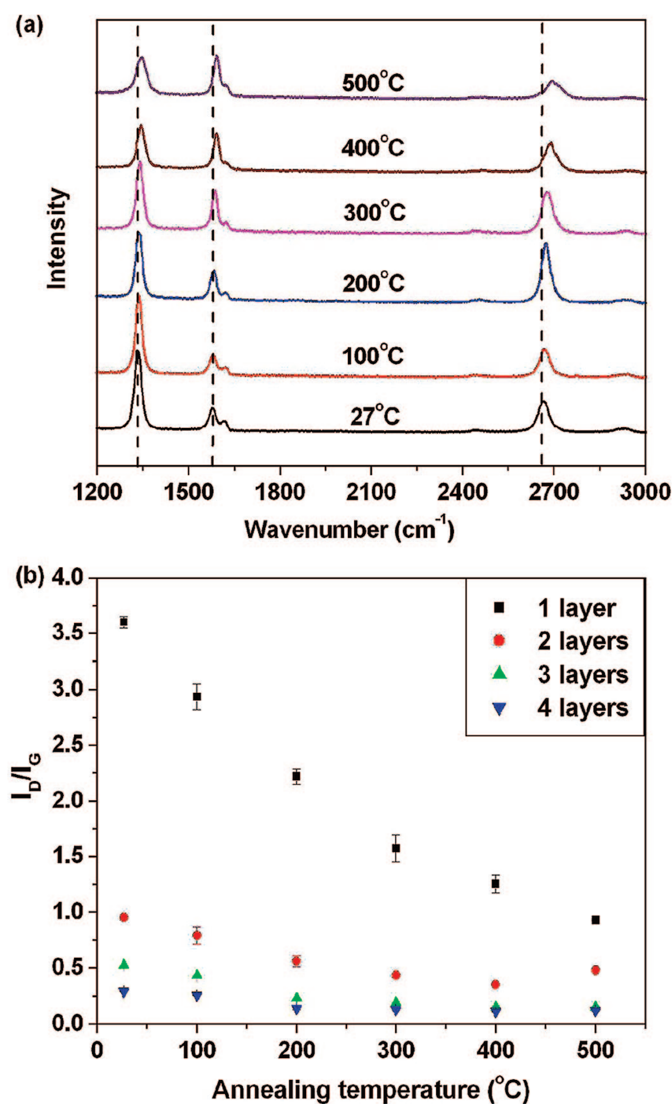

Figure 4. (a) Raman spectra of single layer graphene coated by 5 nm SiO_2 and annealed at different temperature. (b) The intensity ratio of D band and G band (I_D/I_G) of graphene sheets with one to four layers (coated with SiO_2) after annealing at different temperature. The I_D/I_G (defects) decreased significantly upon annealing.

stress on graphene should be biaxial. The biaxial compressive stress on graphene can be estimated from the shift of Raman E_{2g} phonon with the following analysis.

For a hexagonal system, the strain ϵ induced by an biaxial stress σ can be expressed as[35,36]

$$\begin{bmatrix}\varepsilon_{xx}\\ \varepsilon_{yy}\\ \varepsilon_{zz}\\ \varepsilon_{yz}\\ \varepsilon_{zx}\\ \varepsilon_{xy}\end{bmatrix}=\begin{bmatrix}S_{11} & S_{12} & S_{13} & & & \\ S_{12} & S_{11} & S_{13} & & & \\ S_{13} & S_{13} & S_{33} & & & \\ & & & S_{44} & & \\ & & & & S_{44} & \\ & & & & & 2(S_{11}-S_{12})\end{bmatrix}\begin{bmatrix}\sigma\\ \sigma\\ 0\\ 0\\ 0\\ 0\end{bmatrix} \quad (1)$$

with the coordinate x and y in the graphite/graphene plane and with z perpendicular to the plane, so that $\varepsilon_{xx} = \varepsilon_{yy} = (S_{11}+S_{12})\sigma$, $\varepsilon_{zz} = 2S_{13}\sigma$, $\varepsilon_{yz} = \varepsilon_{zx} = \varepsilon_{xy} = 0$.

With all shear components of strain equal to zero, the secular equation of such system can be written as

$$\begin{vmatrix}A(\varepsilon_{xx}+\varepsilon_{yy})-\lambda & B(\varepsilon_{xx}-\varepsilon_{yy})\\ B(\varepsilon_{xx}-\varepsilon_{yy}) & A(\varepsilon_{xx}+\varepsilon_{yy})-\lambda\end{vmatrix}=0 \quad (2)$$

where $\lambda = \omega_\sigma^2 - \omega_0^2$, with ω_σ and ω_0 being the frequencies of Raman E_{2g} phonon under stressed and unstressed conditions.

There is only one solution for this equation

$$\lambda = A(\varepsilon_{xx}+\varepsilon_{yy}) = 2A\varepsilon_{xx} = 2A(S_{11}+S_{12})\sigma \quad (3)$$

Therefore,

$$\omega_\sigma-\omega_0=\frac{\lambda}{\omega_\tau+\omega_0}\approx\frac{\lambda}{2\omega_0}=\frac{A(S_{11}+S_{12})\sigma}{\omega_0}=\alpha\sigma \quad (4)$$

where $\alpha = A(S_{11} + S_{12})/\omega_0$ is the stress coefficient for Raman shift.

Using $A = -1.44 \times 10^7$ cm^{-2}[35] and graphite elastic constants $S_{11} = 0.98 \times 10^{-12}$ Pa^{-1} and $S_{12} = -0.16 \times 10^{-12}$ Pa^{-1},[37] and ω_0= 1580 cm^{-1}, the stress coefficient α is estimated to be 7.47 cm^{-1}/GPa. The estimated stress on single layer graphene with annealing temperature is shown in Figure 5d. The compressive stress on graphene was as high as ~2.1 GPa after depositing SiO_2 and annealing at 500 °C, and the stress on single layer graphene in our experiment can be fitted by the following formula:

$$\sigma = -0.155 + (2.36\times10^{-3})T + (5.17\times10^{-6})T^2 \quad (5)$$

where σ is the compressive stress in GPa and T is temperature in °C. The appearance of such large stress is mainly because graphene sheets are very thin (0.325 nm in thickness for single layer graphene),[38] so that they can be easily compressed or expanded. It has been reported that even the very weak van der Waals interaction can produce large stress on the single-wall carbon nanotubes.[25] We have also introduced tensile stress onto graphene by depositing a thin cover layer of silicon. The G band of graphene red-shifted by ~5 cm^{-1} after silicon deposition, which corresponds to a tensile stress of ~0.67 GPa on graphene sheet. We suggest that tensile stress can be also achieved by depositing other materials with larger lattice constants than graphene. In combination with annealing, both compressive and tensile stress can be introduced and modified in graphene in a controllable manner. The stressed graphene may have very important applications as the properties of graphene (optical and electronic properties) can be adjusted by stress, where stress studies in CNTs have already set good examples,[21−25] for instance, the bandgap of CNTs can be tuned by strain with a parameter of 100 meV per 1% strain.[22] Stress engineering using SiGe alloy has already been used in the IC fabrication to improve the device performance.

Figure 6a shows the optical image of a graphene sheet with one-, two-, three-, four-, five-, and six-layer

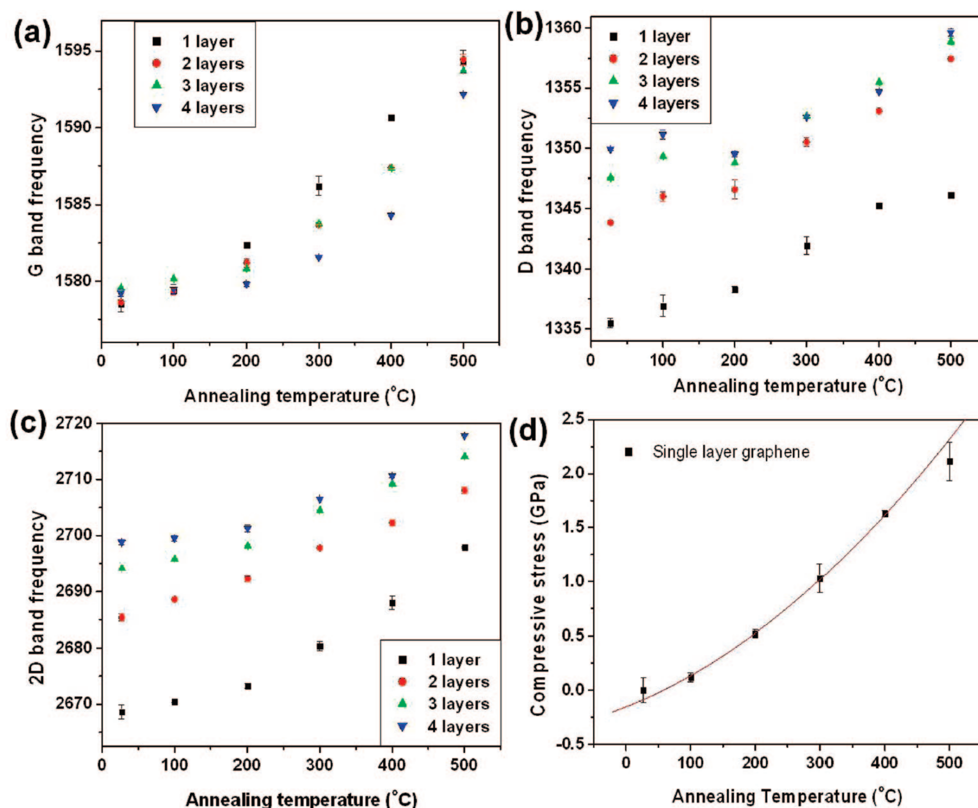

Figure 5. The Raman peak frequency of G band (a), D band (b), and 2D band (c) of graphene sheets with one to four layers (coated with SiO_2) after annealing at different temperature. Blue shifts of all the Raman bands were observed after annealing, which were attributed to the strong compressive stress on graphene. (d) Magnitude of compressive stress on single layer graphene controlled by annealing temperature. The red line is a curve fit to the experimental data.

regions, as denoted by the numbers on the image. After annealing at 600 °C for 30 min, the thinner part of the graphene sheet (regions 1−3) disappeared because of oxidation. However, the thicker part (regions 4−6) still remained, and the thicknesses were reduced to two, three, and four layers, as shown in Figure 6b. The thickness of different regions before and after annealing is determined by a combination of Raman imaging (Figure 6panels c and d) and contrast imaging (Figure 6 panels e and f).[39] Optical spectroscopic imaging techniques have a clear advantage in this case over other techniques, such as atomic force microscopy (AFM), in determining the layer thickness, as AFM does not work properly because of the presence of the SiO_2 top layer on the graphene. Although the exact mechanism of graphene annihilation is unknown, it is most likely due to oxidation of carbon by oxygen diffused through the SiO_2 cover layer from the ambient air as the thickness of the graphenes does not change when annealing is carried out in vacuum. Figure 7 shows the Raman spectra of the remained two and four layers graphene. The D band in both spectra is very weak, indicting the high quality of graphene sheets after thickness modification. This result suggests that annealing in the presence of oxygen provides a practical

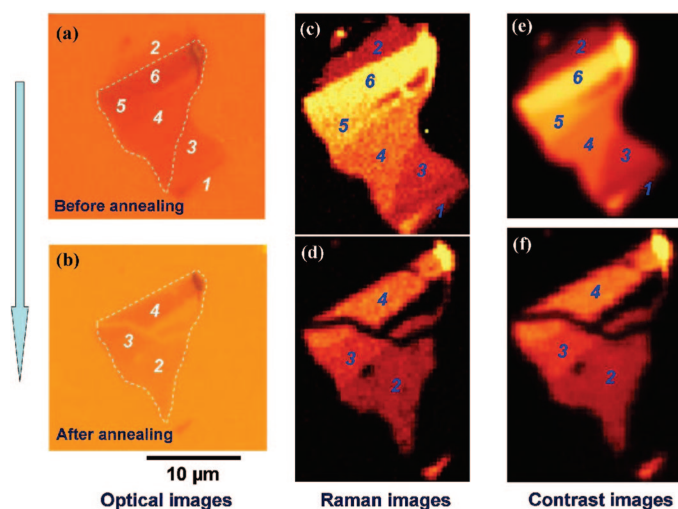

Figure 6. Optical images of a graphene sheet with one-, two-, three-, four-, and six-layer regions before (a) and (b) after annealing at 600 °C for 30 min; Raman (G band intensity) images of the same graphene before (c) and after (d) annealing; contrast images of the same graphene before (e) and after (f) annealing. The one- to three-layer regions disappeared after annealing, while the four- to six-layer regions remained. The thicknesses of three remained regions were two, three, and four layers determined by Raman and contrast imaging.

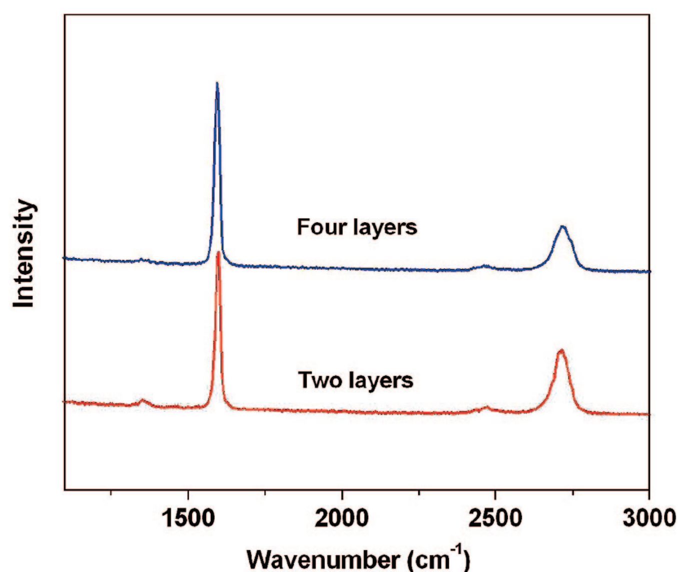

Figure 7. Raman spectra of the two- and four-layer graphene after thickness modification.

method of manipulating the graphene thickness in a controllable manner. For example, a local heating technique may be used to either induce the stress or reduce the thickness selectively, opening another avenue for fabricating graphene-based devices.

CONCLUSION

In summary, we have used Raman spectroscopy and microscopy to investigate the influence of top-gate insulator (5 nm SiO_2) on graphene sheets mainly on two important aspects, defects and stress. The results show that defects were introduced in graphene sheets during deposition and the amounts of defects increase as the graphene thickness decreases. After annealing, the defects in graphene can be greatly reduced. Moreover, significant Raman shifts of all the graphene bands were observed after annealing, which was attributed to the compressive stress on graphene. Importantly, the stress can be controlled by the annealing temperature, which maybe used to tune the optical and electronic properties similar to what has been observed in CNTs. Finally, the graphene thickness can be modified in a controllable manner using annealing. Our findings provide useful information critical to graphene device engineering and fabrication.

EXPERIMENTAL SECTION

The graphene samples were prepared by micromechanical cleavage and transferred to Si wafer substrate with a 300 nm SiO_2 cap layer.[1] Optical microscopy was used to locate the graphene sheet and the thickness was further confirmed by contrast[39] and Raman spectra/image. A 5 nm SiO_2 top layer was deposited by PLD with a 248 nm KrF pulsed laser. The laser power used was very weak (~200 mJ and repetition rate of 10 Hz) to achieve the slow and smooth deposition (1Å/min) and ellipsometry was used to measure the total thickness of SiO_2. The SiO_2 thickness on the Si substrate was 303.5 ± 0.5 nm before deposition and 308.5 ± 0.5 nm after deposition, indicating that the thickness of the top SiO_2 layer was 5 nm. The sample was annealed in a tube furnace at different temperatures for 30 min.

The Raman spectra were recorded with a WITEC CRM200 Raman system with a double-frequency Nd:YAG laser (532 nm) as excitation source. The laser power at sample is below 0.1 mW to avoid laser-induced heating. The contrasts of graphene are obtained by the following calculation: $C(\lambda) = (R_0(\lambda) - R(\lambda))/R_0(\lambda)$, where $R_0(\lambda)$ is the reflection spectrum from the SiO_2/Si substrate and $R(\lambda)$ is the reflection spectrum from the graphene sheet, which is illuminated by normal white light.[39] For Raman/contrast image, the sample was placed on an $x-y$ piezostage and scanned under the illumination of laser/white light. The Raman/reflection spectra from every spot of the sample were recorded. The stage movement and data acquisition were controlled using ScanCtrl Spectroscopy Plus software from WITec GmbH, Germany. Data analysis was done using WITec Project software. A 100× objective lens with a NA = 0.95 was used both in the Raman and reflection experiments, and the spot size of 532 nm laser and white light were estimated to be 500 nm and 1 μm, respectively.

REFERENCES AND NOTES

1. Novoselov, K. S.; Geim, A. K.; Morozov, S. V.; Jiang, D.; Zhang, Y.; Dubonos, S. V.; Grigorieva, I. V.; Firsov, A. A. Electric Field Effect in Atomically Thin Carbon Films. *Science* **2004**, *306*, 666–669.
2. Novoselov, K. S.; Geim, A. K.; Morozov, S. V.; Jiang, D.; Katsnelson, M. I.; Grigorieva, I. V.; Dubonos, S. V.; Firsov, A. A. Two-dimensional Gas of Massless Dirac Fermions in Graphene. *Nature* **2005**, *438*, 197–200.
3. Zhang, Y. B.; Tan, Y. W.; Stormer, H. L.; Kim, P. Experimental Observation of the Quantum Hall Effect and Berry's Phase in Graphene. *Nature* **2005**, *438*, 201–204.
4. Geim, A. K.; Novoselov, K. S. The Rise of Graphene. *Nat. Mater.* **2007**, *6*, 183–191.
5. Han, M. Y.; Ozyilmaz, B.; Zhang, Y. B.; Kim, P. Energy Band-Gap Engineering of Graphene Nanoribbons. *Phys. Rev. Lett.* **2007**, *98*, 206805-1–206805-4.
6. Castro, E. V.; Novoselov, K. S.; Morozov, S. V.; Peres, N. M. R.; Lopes dos Santos, J. M. B.; Nilsson, J.; Guinea, F.; Geim, A. K.; Castro Neto, A. H. Biased Bilayer Graphene: Semiconductor with a Gap Tunable by Electric Field Effect. *Phys. Rev. Lett.* **2007**, *99*, 216802-1–216802-4.
7. Latil, S.; Henrard, L. Charge Carriers in Few-layer Graphene Films. *Phys. Rev. Lett.* **2006**, *97*, 036803-1–036803-4.
8. Zhang, Y.; Jiang, Z.; Small, J. P.; Purewal, M. S.; Tan, Y. W.; Fazlollahi, J. D.; Chudow, J. D.; Jaszczak, J. A.; Stormer, H. L.; Kim, P. Landau-Level Splitting in Graphene in High Magnetic Fields. *Phys. Rev. Lett.* **2006**, *96*, 136806-1–136806-4.
9. Novoselov, K. S.; McCann, E.; Morozov, S. V.; Fal̓ko, V. I.; Katsnelson, M. I.; Zeitler, U.; Jiang, D.; Schedin, F.; Geim, A. K. Unconventional Quantum Hall Effect and Berry's Phase of 2 pi in Bilayer Graphene. *Nat. Phys.* **2006**, *2*, 177–180.
10. Gu, G.; Nie, S.; Feenstra, R. M.; Devaty, R. P.; Choyke, W. J.; Chan, W. K.; Kane, M. K. Field Effect in Epitaxial Grapheneona Silicon Carbide Substrate. *Appl. Phys. Lett.* **2007**, *90*, 253507-1–253507-3.
11. Huard, B.; Sulpizio, J. A.; Stander, N.; Todd, K.; Yang, B.; Goldhaber-Gordon, D. Transport Measurements across a Tunable Potential Barrier in Graphene. *Phys. Rev. Lett.* **2007**, *98*, 236803-1–236803-4.
12. Ozyilmaz, B.; Jarillo-Herrero, P.; Efetov, D.; Abanin, D. A.; Levitov, L. S.; Kim, P. Electronic Transport and Quantum Hall Effect in Bipolar Graphene p-n-p Junction. *Phys. Rev. Lett.* **2007 99**, 166804-1–166804-4.
13. Cheianov, V. V; Fal̓ko, V. I. Selective Transmission of Dirac Electrons and Ballistic Magnetoresistance of n-p Junctions

in Graphene. *Phys. Rev. B* **2006**, *74*, 041403(R)-1041403(R)-4.
14. Cheianov, V. V.; Falḱo, V.; Altshuler, B. L. The Focusing of Electron Flow and a Veselago Lens in Graphene p-n Junctions. *Science* **2007**, *315*, 1252–1255.
15. Katsnelson, M. I.; Novoselov, K. S.; Geim, A. K. Chiral Tunnelling and the Klein Paradox in Graphene. *Nat. Phys.* **2006**, *2*, 620–625.
16. Wehling, T. O.; Novoselov, K. S.; Morozov, S. V.; Vdovin, E. E.; Katsnelson, M. I.; Geim, A. K.; Lichtenstein, A. I. Molecular Doping of Graphene. *Nano Lett.* **2008**, *8*, 173–177.
17. Hwang, E. H.; Adam, S.; Das Sarma, S; Geim, A. K. Transport in Chemically Doped Graphene in the Presence of Adsorbed Molecules. *Phys. Rev. B* **2007**, *76*, 195421-1–195421-6.
18. Ostrovsky, P. M.; Gornyi, I. V.; Mirlin, A. D. Electron Transport in Disordered Graphene. *Phys. Rev. B* **2006**, *74*, 235443-1–235443-20.
19. Pereira, Vitor, M.; Guinea, F.; Lopes dos Santos, J. M. B.; Peres, N. M. R.; Castro Neto, A. H. Disorder Induced Localized States in Graphene. *Phys. Rev. Lett.* **2006**, *96*, 036801-1–036801-4.
20. Yu, M. F.; Lourie, O.; Dyer, M. J.; Moloni, K.; Kelly, T. F.; Ruoff, R. S. Strength and Breaking Mechanism of Multiwalled Carbon Nanotubes under Tensile Load. *Science* **2000**, *287*, 637–640.
21. Maiti, A.; Svizhenko, A.; Anantram, M. P. Electronic Transport through Carbon Nanotubes: Effects of Structural Deformation and Tube Chirality. *Phys. Rev. Lett.* **2002**, *88*, 126805-1–126805-4.
22. Minot, E. D.; Yaish, Y.; Sazonova, V.; Park, J. Y.; Brink, M.; McEuen, P. L. Tuning Carbon Nanotube Band Gaps with Strain. *Phys. Rev. Lett.* **2003**, *90*, 156401-1–156401-4.
23. Tombler, T. W.; Zhou, C.; Alexseyev, L.; Kong, J.; Dai, H.; Liu, L.; Jayanthi, C. S.; Tang, M.; Wu, S. Reversible Electromechanical Characteristics of Carbon Nanotubes under Local-Probe Manipulation. *Nature* **2000**, *405*, 769–772.
24. Heyd, R.; Charlier, A.; McRae, E. Uniaxial-Stress Effects on the Electronic Properties of Carbon Nanotubes. *Phys. Rev. B* **1997**, *55*, 6820–6824.
25. Son, H.; Samsonidze, G. G.; Kong, J.; Zhang, Y. Y.; Duan, X. J.; Zhang, J.; Liu, Z. F. Strain and Friction Induced by Van der Waals Interaction in Individual Single Walled Carbon Nanotubes. *Appl. Phys. Lett.* **2007**, *90*, 253113-1–253113-3.
26. Mintmire, J. W.; White, C. T. Electronic and Structural Properties of Carbon Nanotubes. *Carbon* **1995**, *33*, 893–902.
27. Ferrari, A. C.; Meyer, J. C.; Scardaci, V.; Casiraghi, C.; Lazzeri, M.; Mauri, F.; Piscanec, S.; Jiang, D.; Novoselov, K. S.; Roth, S.; et al. Raman Spectrum of Graphene and Graphene Layers. *Phys. Rev. Lett.* **2006**, *97*, 187401-1–187401-4.
28. Graf, D.; Molitor, F.; Ensslin, K.; Stampfer, C.; Jungen, A.; Hierold, C.; Wirtz, L. Spatially Resolved Raman Spectroscopy of Single- and Few-Layer Graphene. *Nano Lett.* **2007**, *7*, 238–242.
29. Thomsen, C.; Reich, S. Double Resonant Raman Scattering in Graphite. *Phys. Rev. Lett.* **2000**, *85*, 5214–5217.
30. Barros, E. B.; Demir, N. S.; Souza Filho, A. G.; Mendes Filho, J.; Jorio, A.; Dresselhaus, G.; Dresselhaus, M. S. Raman Spectroscopy of Graphitic Foams. *Phys. Rev. B* **2005**, *71*, 165422-1–165422-5.
31. Gupta, A.; Chen, G.; Joshi, P.; Tadigadapa, S.; Eklund, P. C. Raman Scattering from High-Frequency Phonons in Supported n-Graphene Layer Films. *Nano Lett.* **2006**, *6*, 2667–2673.
32. Yan, J.; Zhang, Y. B.; Kim, P.; Pinczuk, A. Electric Field Effect Tuning of Electron-phonon Coupling in Graphene. *Phys. Rev. Lett.* **2007**, *98*, 166802-1–166802-4.
33. Pisana, S.; Lazzeri, M.; Casiraghi, C.; Novoselov, K. S.; Geim, A. K.; Ferrari, A. C.; Mauri, F. Breakdown of the Adiabatic Born-Oppenheimer Approximation in Graphene. *Nat. Mater.* **2007**, *6*, 198–201.
34. Das, A.; Pisana, S.; Piscanec, S.; Chakraborty, B.; Saha, S. K.; Waghmare, U. V.; Yiang, R.; Krishnamurhthy, H. R.; Geim, A. K.; Ferrari, A. C.; *et al.* Monitoring Dopants by Raman Scattering in an Electrochemically Top-Gated Graphene Transistor. *Nat. Nanotechnol.* **2008**, *3*, 210–215.
35. Sakata, H.; Dresselhaus, G.; Dresselhaus, M. S.; Endo, M. Effect of Uniaxial Stress on the Raman Spectra of Graphite Fibers. *J. Appl. Phys.* **1988**, *63*, 2769–2772.
36. Ni, Z. H.; Chen, W; Fan, X. F.; Kuo, J. L.; Yu, T.; Wee, A. T. S.; Shen, Z. X. Raman Spectroscopy of Epitaxial Grapheneona SiC Substrate. *Phys. Rev. B* **2008**, *77*, 115416-1–115416-6.
37. Dresselhaus, M. S.; Dresselhaus, G.; Sugihara, K.; Spain, I. L.; Goldberg, H. A. In *Graphite Fibers and Filaments*; Springer: Heidelberg, 1988; pp 85−123..
38. Dresselhaus, M. S.; Dresselhaus, G.; Eklund, P. C. *Science of Fullerenes and Carbon Nanotubes*; Academic Press: San Diego, CA, 1996; p 965.
39. Ni, Z. H.; Wang, H. M.; Kasim, J.; Fan, H. M.; Yu, T.; Wu, Y. H.; Feng, Y. P.; Shen, Z. X. Graphene Thickness Determination using Reflection and Contrast Spectroscopy. *Nano Lett.* **2007**, *7*, 2758–2763.